Spatial soliton laser: Localized structures in a laser with a saturable absorber in a self-imaging resonator

V. B. Taranenko, K. Staliunas, and C. O. Weiss
Physikalisch Technische Bundesanstalt, 38116 Braunschweig, Germany
(Received 7 February 1997)

We demonstrate theoretically and experimentally the manipulation of spatial localized structures (spatial solitons) of a laser with saturable absorber in a self-imaging resonator. We show the on-off bistability of the solitons, their movement by phase gradient forces, the parameters of their existence, the limits of their stability, and periodic soliton nucleation and dynamics. [S1050-2947(97)04908-1]

PACS number(s): 42.65.Sf, 42.60.Mi, 42.65.Tg

I. INTRODUCTION

Spatial localized structures (LS's), or spatial solitons are presently of interest in optics because of their potential applications for parallel information processing purposes, such as optical pattern recognition, classification, and parallel information storage. Up to now, such localized structures have been theoretically predicted in the following systems: (1) externally driven Fabry-Pérot resonators with focusing media inside (optically bistable devices) [1]; (2) laser systems with saturable absorber [2]; (3) optical parametric oscillators [3]. Experimentally, LS's have been demonstrated in a laser with saturable absorber [4] and in a corresponding system, where the gain and loss elements in the resonator were photorefractive crystals [5]. Apart from this, LS's have been experimentally realized in electro-optical systems, such as liquid-crystal light valves [6], which are, however, not pure ''all optical'' systems.

Here, we work with spatial solitons in a laser with gain element and saturable absorber in conjugated planes of the resonator. The shape of the spatial soliton is given not by the resonator geometry, but by a balance between nonlinearities on one side, and diffraction and/or diffusion on the other side. The spatial soliton can move freely in transverse direction throughout the laser aperture and the soliton can be bistable with respect to switching it on and off. This means that a soliton can be ''written'' anywhere in the laser cross section, thus providing a spatial memory function.

We show how a spatial soliton can be caused to move by gradient forces, in particular by phase gradients in the cross section of the laser aperture. This can, e.g. be used to trap a soliton at a desired location, providing a means for pattern recognition [7], or to manipulate solitons otherwise. Stability limits, writing and erasing of solitons, as well as dynamic regimes of solitons are shown.

The specific properties of the solitons in the system used (laser with saturable absorber in conjugated planes of a self-imaging resonator) are discussed as opposed to a corresponding laser in a plane mirror resonator [2]. The spatial soliton in this (conjugated plane) configuration is shown to be a spatial analogue of the temporal pulse emitted by a passively mode-locked laser.

We start with the description of the experimental setup, and the corresponding theoretical model (Sec. II). In Sec. III evidence of spatial solitons is given. Section IV gives the analysis of existent parameters and stability limits of the spatial LS's. In Sec. V some dynamical peculiarities are reported, such as the drift of localized structures due to phase gradients, soliton gluing to the edges of the laser aperture, switching on and off by means of external injection, and also periodic dynamics of spatial solitons under continuous injection and a phase gradient.

II. EXPERIMENT AND MODEL

A. Experimental setup

A self-imaging resonator configuration is used for a dye laser with bacteriorhodopsin (BR) as a saturable absorber. The gain element (dye cell) and the saturable absorber are placed in Fourier conjugate planes of the resonator. In order to give freedom for pattern formation this resonator provides a large area near the mirrors and small beam diameter in the center at the gain element. A scheme of experimental setup is shown in Fig. 1.

We use a solution of 6-aminophenolynon in ethyl alcohol as the gain element in order to match the spectral absorption band of BR. The dye solution flows inside a cuvette located in the central part of the resonator. The dye cell is pumped by the second harmonic (at 532 nm) of a passively Q-switched Nd:YAG (neodymium-doped yttrium aluminum garnet) laser operating in a pulse-periodic regime with a repetition rate of 12.5 Hz. Typical values for the pumping pulses are 2 mJ (pulse energy) and 15 ns (pulse width). The

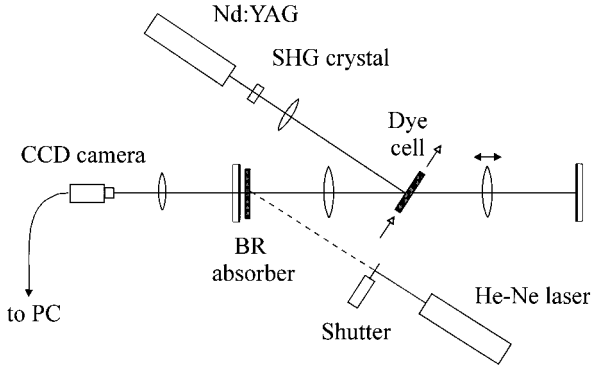

FIG. 1. Experimental setup.

pump beam irradiates the active cell at a small angle (~8°) with respect to the resonator axis. The pumped area of the dye cell is 0.2 mm diameter for the focused pump beam and 1 mm for an unfocused beam. At that pumping condition, the unsaturated single pass gain of the dye cell reaches more than 100.

A cell with BR absorber is placed near one resonator mirror. A water-glycerol suspension of genetically modified BR-D96N [8] is used as the saturable absorber. BR is a photoactive energy converting molecule [9] having a large extinction coefficient of 63 000 $M^{-1}\,cm^{-1}$ at 568 nm. Nonlinear materials based on BR and its genetically modified analogues are easily saturated (10 mW/cm^2) and are extremely stable against thermal and photochemical degradation [10]. In order to increase the photoresponse time of BR-D96N (up to around 1 s) and thereby integrate the laser pulses, the suspension was buffered at *p*H 9. The unsaturated transmission of the BR absorber is chosen to be 0.028 at 532 nm.

The change of the intracavity BR absorber transmission is initiated by an additional (bleaching) unfocused beam of a He-Ne laser (TEM_{00}, $\lambda=633$ nm) controlled by a shutter. The linear resonator length is fixed (365 mm) and equals $4f$ (where f is the focal length of the lenses) while the distance between the active element and one of the intracavity lenses can be varied. The transverse structure of the laser emission in the near field is monitored by a CCD camera connected to a computer.

B. Theoretical model

Here, we derive the theoretical model for lasers with saturable absorber in a self-imaging resonator based on existing models for such a laser with plane resonator. Such a model has been used in Ref. [2] to study the localized structures in lasers with saturable absorber in plane resonators:

$$\partial_t A=\frac{pA}{1+|A|^2/a_p}-\frac{\beta_0 A}{1+|A|^2/a_s}-\alpha A+(d_{\mathrm{Re}}+id_{\mathrm{Im}})\nabla^2 A. \tag{1}$$

Here, p is the gain parameter, a_p is the gain saturation intensity, β_0 is the maximum value of the nonlinear absorption, a_s is the absorption saturation intensity, α is the linear loss, and d_{Re} and d_{Im} are the diffusion and diffraction coefficients. The order parameter $A(\vec{r},t)$ is proportional to the envelope of the optical field in the two-dimensional transverse plane $\vec{r}=(x,y)$, and depends on time normalized to the photon round-trip time. Using this normalization, the diffraction coefficient is $d_{\mathrm{Im}}=L/(2k)$, where L is the full resonator length (twice the linear resonator length), and k is the wave number of the radiation. Diffusion coefficient d_{Re} is related to the spatial frequency filtering, and will be discussed below.

Equation (1) was derived, using adiabatic elimination of the fast atomic variables, from the Maxwell-Bloch equation system (including two-level amplifying and also absorbing atoms). It assumes that the population inversion of the amplifying medium, and that of the nonlinear absorber, relaxes infinitely fast in comparison with the optical field. In order to account for the effects of inertia of absorber, the underlying Eq. (1) can be modified to yield

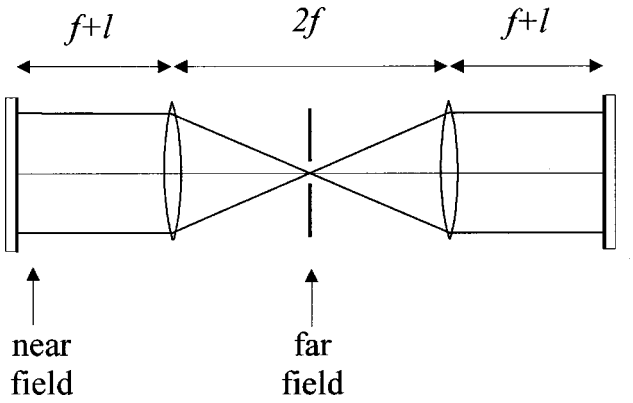

FIG. 2. Sketch of the quasi-self-imaging resonator used in experiment. The deviation from the self-imaging length is l.

$$\partial_t A=\frac{pA}{1+|A|^2/a_p}-(\alpha+\beta)A+(d_{\mathrm{Re}}+id_{\mathrm{Im}})\nabla^2 A, \tag{2a}$$

$$\partial_t \beta=\gamma(\beta_0-\beta-\beta|A|^2/a_s), \tag{2b}$$

which in the limit of fast absorber $\gamma\to\infty$ coincides with Eq. (1).

Equations (1) and (2) describe light matter interaction phenomena of lasers with saturable absorber. These models, however, are valid only in the paraxial approximation corresponding to a plane resonator. For resonator configurations different from planar, the system has particular properties which have to be taken into account by modifying Eqs. (1) and (2). In the following, we derive the model for our self-imaging resonator configuration, based on Eqs. (1) and (2).

The linear parts of Eq. (1) can be retrieved by calculating the light rays in geometrical optics. The ray inclined by an angle θ to the optical axis of the plane mirror resonator has a larger optical path in one round-trip in the resonator compared with the ray directed parallel to the optical axis. The change of the optical path length is $\Delta L=L\theta^2/2$, for small angles θ. Relating the angle with the components of the wave number parallel and perpendicular to the optical axis of the resonator: $\theta=k_\perp/k$, one obtains the dispersion relation for the planar resonator, $\omega_{k_\perp}=Lk_\perp^2/(2k)$ (we recall that the frequency is normalized to the free-spectral range). This leads to the diffraction term in Eq. (1) with diffraction coefficient $d_{\mathrm{Im}}=L/(2k)$.

The dispersion relation (thus diffraction coefficient in the order-parameter equations) can be obtained directly from the $ABCD$ matrix [11] analysis. The $ABCD$ matrix for a planar resonator is

$$ABCD=\begin{Vmatrix}1 & L\\ 0 & 1\end{Vmatrix}. \tag{3}$$

The dependence of optical length on the angle θ is given by the nondiagonal element of $ABCD$ matrix $(ABCD)_{12}$, $\Delta L=(ABCD)_{12}\ \theta^2/2$. This leads to the above calculated dispersion relation, and the correct value of diffraction parameter.

The $ABCD$ matrix for our near self-imaging resonator (Fig. 2) is

$$ABCD=\begin{Vmatrix} 1 & 4\cdot l \\ 0 & 1 \end{Vmatrix}. \tag{4}$$

Here, l is the displacement of the plane mirrors from the self-imaging length. For the precisely self-imaging case $l=0$, and $ABCD$ matrix is the unit matrix. This means that a ray with arbitrary position and arbitrary angle to the optical axis returns back to the same position after one round trip. As a consequence, every ray has the same optical length in one round-trip in the resonator. This leads to no dispersion of the resonator; thus to zero diffraction, $d_{\mathrm{Im}}=0$.

For the approximate self-imaging case ($l\neq 0$), the $ABCD$ matrix of our resonator coincides with that for planar resonator of the total length $4l$. Then the order-parameter Eqs. (1) and (2), derived from the planar resonators, are valid also for the case of nearly-self-imaging resonators. The diffraction coefficient for our resonator is $d_{\mathrm{Im}}=2l/k$.

The mathematically rigorous proof of equivalence between the planar and self-imaging resonators will be given elsewhere. We note here that this equivalence has important consequences. As follows, the resonator as used in our experiment can reproduce a planar resonator of extremely (in the limiting case, infinitely) small length. This allows the reader to obtain extremely large Fresnel numbers (aspect ratio) of the system. For instance, the smallest size of the localized structure in the planar resonator is $\Delta x=d_{\mathrm{Im}}^{1/2}=(L\lambda)^{1/2}$, and is limited in optics mainly by the resonator length. In the case of our self-imaging resonator, the minimum size of the LS's could be decreased to zero, if the paraxial approximation would hold.

We note, that for resonators with the length shorter than the self-imaging length, the diffraction coefficient is negative. This means that the optical length for rays at nonzero angle to the optical axis is smaller than that for the rays parallel to the optical axis of the resonator. However, in the absence of the focusing or defocusing nonlinearities the sign of diffraction has no meaning.

As a conclusion, one can use Eqs. (1) or (2) in order to simulate spatiotemporal dynamics of fields of lasers in self-imaging or quasi-self-imaging resonators. The only difference from the planar resonator case is the value of the diffraction coefficient.

There is a requirement for validity of Eqs. (1) and (2) for the nearly-self-imaging case: all the nonlinear processes must occur in the same location of the resonator along its optical axis. This requirement has no meaning in the quasi-planar resonator case, since the field variation along the resonator is negligible there. In our case, the fields vary strongly from the near field to the far field. Let us assume for definitiveness that the near field is generated at the plane mirror of the resonator. Then, the field at the focal point of the resonator is the far field, which is the Fourier transform of the near field. Consequently, there is a difference as to where a nonlinear element is placed. Obviously, nonlinear operators acting on the field in the space domain or in the Fourier domain lead to different results.

It follows then, that the models, Eqs. (1) or (2) are valid if the both nonlinear elements are either in the far-field plane, or in the near-field plane: it is important that the nonlinear operators act on the same domain. The situation in the experiment is different. The nonlinear absorption takes place close to the resonator mirror, the nonlinear amplification of the fields, however, takes place at the focal plane of the resonator. Then Eqs. (2) have to be rewritten to take into account this ''far-field–near-field separation'':

$$\partial_t A(\vec{r},t)=\hat{F}^{-1}\hat{N}(p,a_p)\hat{F}A(\vec{r},t)+(d_{\mathrm{Re}}+id_{\mathrm{Im}})\nabla^2 A(\vec{r},t) -[\alpha+\beta(r,t)]A(\vec{r},t), \tag{5a}$$

$$\partial_t \beta(\vec{r},t)=\gamma(\beta_0(\vec{r})-\beta(\vec{r},t)-\beta(\vec{r},t)|A(\vec{r},t)|^2/a_s). \tag{5b}$$

The $\hat{N}(p,a_p)$ is a nonlinear operator of saturable gain:

$$\hat{N}(p,a_p)A=\frac{pA}{1+|A|^2/a_p} \tag{6}$$

acting on the field variable not in the spatial domains as in Eqs. (1) and (2), but in the Fourier domain. The spatial Fourier transform (and afterwards the inverse Fourier transform) is therefore used in Eq. (5a) to change from the near-field to far-field domain (and vice versa):

$$\hat{F}A=\frac{1}{2\pi}\int\int A(x,y,t)\exp(ik_x x+ik_y y)dx\ dy, \tag{7a}$$

$$\hat{F}^{-1}A=\frac{1}{2\pi}\int\int A(k_x,k_y,t)\exp(-ik_x x-ik_y y)dk_x dk_y. \tag{7b}$$

The (physical) spatial coordinate in the Fourier plane is related with the transverse wave number via $r_F=k_\perp(\lambda f/\pi)$. [A Gaussian beam of width $r_0=(\lambda f/\pi)^{1/2}$ is the same width in the near- and far-field planes.]

Lateral boundary conditions must be added to the Eqs. (5). The iris in the near-field plane is approximated by the corresponding spatial profile of the gain (or losses) $\alpha=\alpha(\vec{r})$. The aperture in the far field (focal plane) results in spatial frequency filtering, and is correspondingly approximated by the profile of losses in the Fourier domain. Assuming a parabolic profile of the gain in the Fourier domain, $\partial_t A(\vec{k}_\perp,t)=-d_{\mathrm{Re}}k^2 A(\vec{k}_\perp,t)$, and converting to the space domain by inverse Fourier transform, one obtains $\partial_t A(\vec{r},t)=d_{\mathrm{Re}}\nabla^2 A(\vec{r},t)$. This means that the diaphragm in the Fourier domain is equivalent to diffusion in the space domain. This latter is the reason why the Laplace operator in (1, 2, 5) has not only an obvious imaginary part (with coefficient d_{Im}) corresponding to diffraction, but also a real part (with coefficient d_{Re}) corresponding to diffusion.

The model (5) is the basis for the numerical analysis in the paper. We used the split-step technique for numerical integration of Eq. (5a). In this technique, the local terms (the linear losses and the nonlinear absorption) are calculated in the space domain, whereas the nonlocal terms (diffraction and diffusion of field, also the gain) are calculated in the spatial wave-vector (Fourier) domain. A fast-Fourier transformation is used to change from the physical space to the spatial wave-vector space in every step of the numerical integration. Spatial grids were used of (128×128) for one- and two-dimensional calculations; the spatial coordinate was nor-

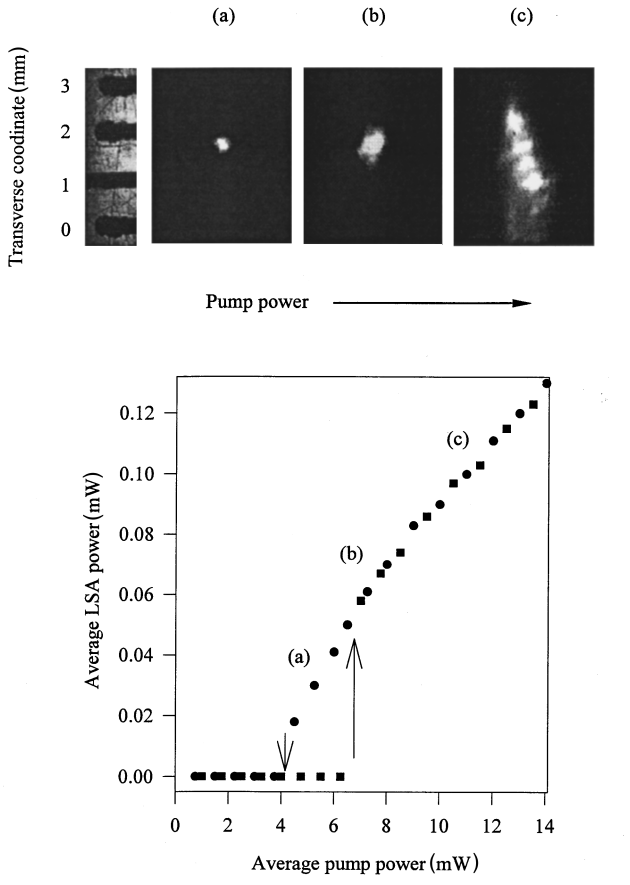

FIG. 3. Experimentally measured hysteresis in the dependence of the laser output on the pump, and the transverse structure of the output laser beam for three fixed pump powers: (a) small size and quasi-Gaussian spatial soliton in the bistable region, (b) intermediate size and super Gaussian soliton at the border between bistability and monostability, and (c) large size structure of strongly structured profile in the monostable region.

malized to the size of the integration region. Equation (5b) was integrated in the spatial domain, since it does not contain any nonlocal terms.

III. EVIDENCE OF LOCALIZED STRUCTURES

A. Experimental evidence of localized structures

The experimentally measured dependence of the average laser output power on the average pump power shown in Fig. 3 exhibits a hysteresis loop (optical bistability). At pump powers corresponding to the bistable region [Fig. 3(a)] the laser emits a small isolated quasi-Gaussian light spot. An increase of pump power leads to an increase of the laser beam cross section, which is accompanied by a change of its shape in the region between the bistable and monostable regime [Fig. 3(b)] and by structuring in the monostability regime [Fig. 3(c)].

The spatial soliton size depends essentially on the pumping area aperture on the dye cell: the larger the pumping area, the smaller the spatial soliton size (compare the spot size for two cases: when the pump beam is focused [Fig. 4(a)] and unfocused [Fig. 4(b)] into the dye cell, respectively). This shows that the spatial soliton size is limited primarily by the

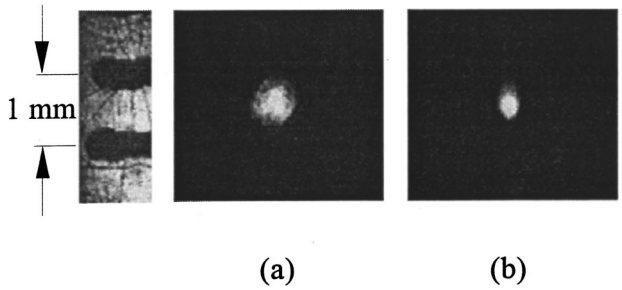

FIG. 4. Experimental observation of the laser spatial soliton structure: (a) for small and (b) for large pump area in the dye cell, illustrating the dependence of soliton size on diffusion.

diffusion coefficient in Eq. (5).

When the pump power is inside the hysteresis range [Fig. 3(a)] the spatial soliton can be switched on by a bleaching light beam incident on the BR absorber. The soliton can be switched on in any plane on the laser cross section, which in our case is limited by the BR absorber cell aperture (10 mm). Figure 5 demonstrates how the single spatial soliton is switched on by the writing laser beam applied in different places of the BR absorber for a short time. (The power of the He-Ne laser beam used for writing was 2 mW, the energy density necessary for writing the LS's was 15 mJ/cm^2.) After the spatial soliton is switched on in a particular place of the laser cross section it remains stable in this position. In other words, the laser possesses spatial multistability: a single bistable spatial soliton can have different stable positions (different spatial states of the laser).

B. Numerical evidence of the localized structures

We confirm the existence of localized structures by numerical integration of Eq. (5). The series of plots in Fig. 6

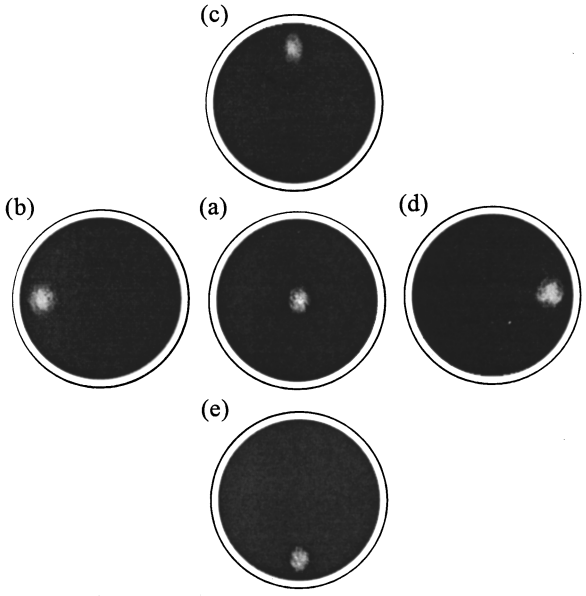

FIG. 5. Positioning of a spatial soliton initiated by an external beam in different places of the laser cross section (the region inside the dark circle is 2.7 mm in diameter). (a) Center, (b) left, (c) up, (d) right, and (e) down.

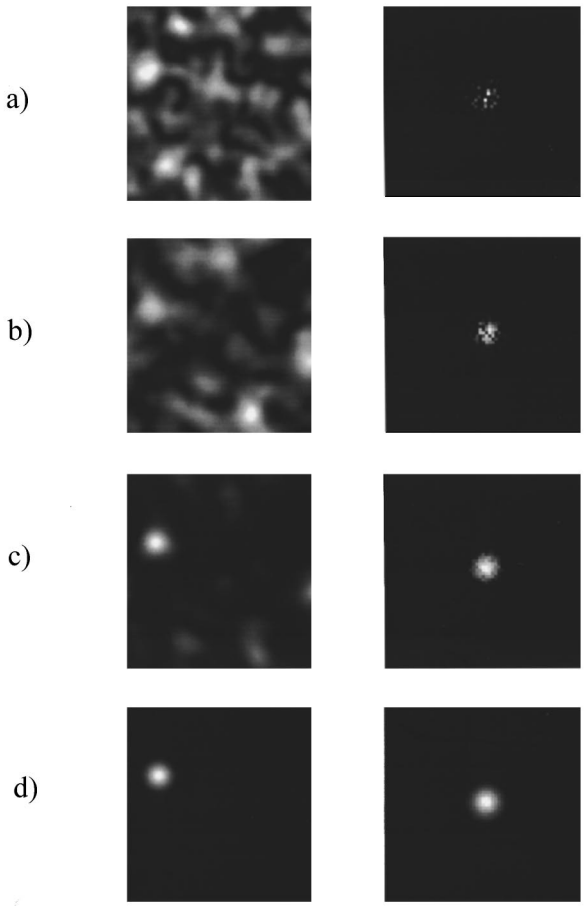

FIG. 6. Evolution of the symmetric stable localized structure from an initial randomly distributed field as obtained by numerical integration of Eq. (5) in the case of two spatial dimensions: left, spatial distributions (near field); right, spatial spectra (far field). The parameters are $d_{\mathrm{Re}}=10^{-3}$, $d_{\mathrm{Im}}=0.25\times10^{-3}$, $p=2$, $a_p=9.82$, $\beta_0=1$, $a_s=0.5$, $\alpha=0$. The plots are given at times (a) $t=2.5$, (b) $t=5.0$, (c) $t=7.5$, (d) $t=10$.

show a LS developing from noise. We started from an initial random distribution of fields [Fig. 6(a)]; the pump parameter was larger than that corresponding to the bistable case (the system is in the monostable regime). In the subsequent evolution, the field grows linearly until the nonlinear regime is reached. In the linear stage of evolution filtering in the spatial Fourier domain was apparent, which leads to the narrowing of the spatial spectrum and consequently to broadening of the spots in the spatial domain [Fig. 6(b)].

In the nonlinear stage of the evolution two physical processes dominate. Due to gain saturation, the spatial spectrum broadens, thus the spots in the near field begin to narrow. The saturation of absorption in the space domain also leads to a narrowing of the spots. Thus these two nonlinear processes ''work in the same direction'' and lead to a formation of an ensemble of symmetric spots [Fig. 6(c)]. The width of the spots is determined by the diffusion and diffraction properties of the resonator (by the diffusion coefficient d_{Re}, which is determined by the width of the aperture in the focal plane of the resonator, and by the diffraction coefficient d_{Im}, which is determined by the difference from the self-imaging length). The spots at this stage of evolution are ''spectrally limited'' in the sense of spatial spectrum.

In the subsequent nonlinear evolution, competition between the spots occur. The spots, although well separated in the space domain, overlap completely in the focal plane. The gain saturation in the focal plane determines the total energy of the radiation. Thus several spots in the spatial domain share the inversion. The more spots in the ensemble, the smaller the average energy (and peak intensity) of the spots. Due to nonlinear absorption, the weaker spots are more strongly discriminated. This leads to competition among the spots. The strongest spot survives in this competition, and a single LS in the form of a symmetric spot finally develops [Fig. 6(d)]. The spot shape is independent of its location, and the location is determined by the initial random distribution. The spots (actually only one spot) can move freely in the transverse plane.

This scenario of developing a single spot in the transverse plane is analogous to the pulse formation in lasers with passive mode locking. In both cases one starts from a random-field distribution in the form of a random ensemble of pulses or spots. In both cases the spectral filtering occurs in the linear stage of the evolution (of frequency and of spatial Fourier spectrum, correspondingly). In both cases only one pulse or spot survives in the nonlinear stage of the evolution. The competition occurs, because several pulses (spots) share a common population inversion. For mode-locked lasers the amplifying medium is relatively slow and the amplification depends on the integral energy. For our pattern forming laser, the spatial spectra of individual pulses overlap in the focal plane, and the amplification again depends on the integral (in space) characteristics of the radiation.

IV. PARAMETERS OF LOCALIZED STRUCTURES

A. Gaussian and/or parabolic expansion

For analytical treatment of single LS's we approximate their profile by a Gaussian function with unknown time-dependent parameters: $A(r,t)=a(t)^{1/2}\exp[-c(t)r^2]$. Inserting this into Eq. (5) one obtains a set of equations for the complex parameters of the LS's. Some assumptions are made allowing the reader to obtain a simple set of equations.

(i) Strong diffusion compared to diffraction: $d_{\mathrm{Re}}\gg d_{\mathrm{Im}}$: This means, that the length of the resonator is precisely tuned to correspond to a self-imaging resonator. This allows the reader to consider the parameters of LS's as real variables.

(ii) Fast saturable absorber: $\gamma\gg1$: this allows the reader to eliminate adiabatically, the absorption variable from Eq. (5b).

(iii) Parabolic profile of the LS's. This allows the reader to simplify the saturating nonlinear terms by a series expansions:

$$\frac{A}{1+|A|^2/a_s}\rightarrow\frac{\sqrt{a}}{1+a\exp(-2cr^2)/a_s}\rightarrow\frac{\sqrt{a}}{1+a/a_s-2acr^2/a_s}$$
$$\rightarrow\frac{\sqrt{a}}{1+a/a_s}\left[1+\frac{2a\ cr^2}{a+a_s}\right]. \tag{8}$$

Using the above assumptions one obtains from Eq. (5):

$$d_t a = -\frac{2\beta_0 a}{1+a/a_s} + \frac{2pa[1+3a/(a_p 4c^2)]}{[1+a/(a_p 4c^2)]^2} - 2\alpha a - 8acd_{\mathrm{Re}}, \tag{9a}$$

$$d_t c = \frac{2\beta_0 ca/a_s}{(1+a/a_s)^2} + \frac{pa/(a_p 2c)}{[1+a/(a_p 4c^2)]} - 4c^2 d_{\mathrm{Re}}. \tag{9b}$$

The system (9) is still too complicated to obtain analytically tractable steady-state solutions, however, its analysis is useful to obtain insight into the process of formation of the LS's.

The system (9) leads to singular solutions if diffusion is absent, $d_{\mathrm{Re}}=0$. Equation (9b) results in a continuous increase of the parameter $c(t)$ (inverse width of the LS), which means that the structure shrinks continuously. For $p>\alpha+\beta_0/(1+a/a_s)$ the amplitude $a(t)$ grows correspondingly, which leads to formation of an unphysical singularity.

The latter can be understood from the following considerations: The saturating absorption leads to narrowing of the LS. The saturating gain would lead to a broadening of the structure if it would occur in the space domain. Such a balance of saturation absorption and saturating gain leads to the formation of the spatial solitons in the quasiplanar cavity lasers [2]. However, in our case the saturating gain occurs in the Fourier plane, and the broadening of the structure in the Fourier domain leads to narrowing of the corresponding structure in the spatial domain. Thus, both nonlinear processes narrow the LS, and develop a singularity if no other physical phenomena balance this ''double'' narrowing. The balance in our model comes from the diffusion, as Eq. (9b) shows.

To demonstrate the counterbalance between nonlinearities on one side, and diffusion on the other side, we plot in Fig. 7 the vector field generated by Eqs. (9). The arrows in Fig. 7 indicate the direction of temporal evolution of the state vector of the system (9) [horizontal, inverse width $c(t)$, of LS's, vertical, peak intensity $a(t)$]. Figure 7(a) represents the below threshold case: the axis $a=0$ (corresponding to trivial solution) is absolutely attracting.

Increase of the pump parameter leads to the saddle-node bifurcation as shown in Fig. 7(b). The node point corresponds to the parameters of the stable LS's. Due to the presence of the saddle point the node is not absolutely attracting: the trivial zero solution is also possible. In this regime a LS appears via subcritical bifurcation, and thus is bistable. One has then a possibility to write and erase a LS.

Further increase of the pump $p>\alpha+\beta_0$ results in monostability, as shown in Fig. 7(c). The LS develops from arbitrary initial conditions. In this regime one cannot erase the LS's: the trivial zero solution is linearly unstable.

The evolution diagram leads to an understanding of the qualitative behavior of the system. To determine the parameters of the LS's one can solve Eq. (7) numerically. However, we present rather the results of the numerical integration of the initial partial differential Eqs. (5) to determine the parameters of the LS's.

B. Numerical integration

We solve numerically, the initial partial differential equations (5) to determine the parameters and stability limits of the LS's without the approximations used to derive Eqs. (9). The calculations were carried out for one dimension due to restrictions of computational facilities [a few runs have been done also for two-dimensional cases (see, e.g., Fig. 6), however, this does not show qualitative differences].

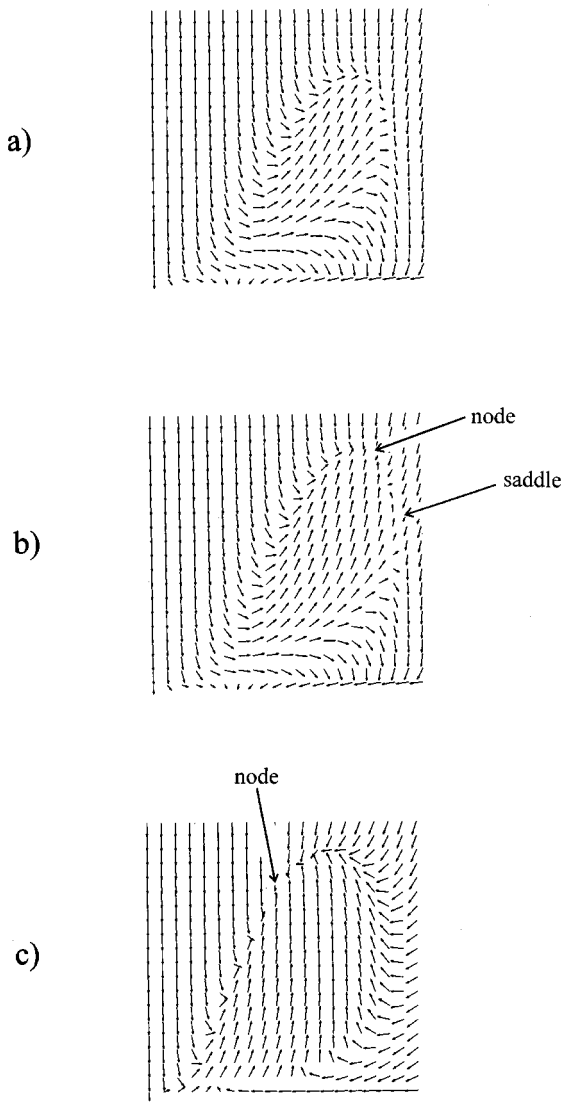

FIG. 7. The vector field of evolution of parameters of the spatial soliton [amplitude $a(t)$, in the vertical direction; and inverse width $c(t)$, in the horizontal direction] as given by parabolic expansion (7). (a) Below the threshold, $p=0.75$, $d_{\mathrm{Re}}=0.127$; (b) corresponding to bistability, $p=0.79$, $d_{\mathrm{Re}}=0.13$; and (c) in the monostable regime, $p=1.6$, $d_{\mathrm{Re}}=0.29$. Other parameters are $a_p=1$, $a_s=1$; amplitude $a(t)$ varies from 0 to 8.4; and inverse width $c(t)$, from 0 to 1.4 in all three cases.

In numerical calculations we use a small but nonzero value of the diffraction parameter $d_{\mathrm{Im}}=10^{-4}$. In the corresponding experiment, this means a small deviation of the resonator length from the self-imaging length. In Fig. 8 the width of the localized structure versus gain is plotted. The four curves in the figure correspond to four different values of diffusion (different radii of apertures in the focal plane). Towards small pump values, the LS's die at the end of the corresponding curves. Towards larger pump values, the LS's begin to pulsate periodically at the end of the cor-

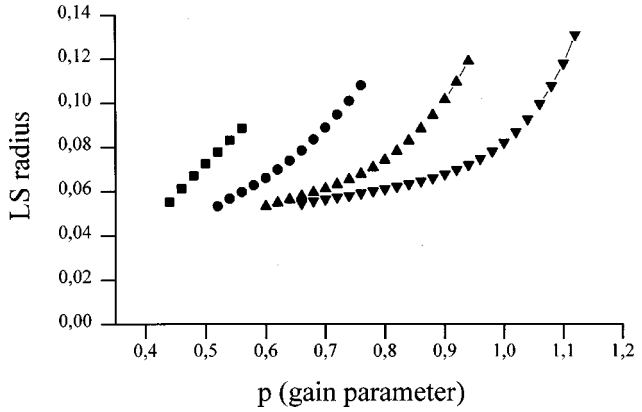

FIG. 8. The width of the stable LS versus pump parameter for four different values of diffusion coefficient (diameter of the aperture in the focal plane) as obtained by numerical integration of Eq. (5) in the case of one spatial dimension. The parameters are $d_{\mathrm{Im}}=10^{-4}$, $p=2$, $a_p=7.83$, $\beta_0=1$, $a_s=1$, and $\alpha=0$. The value of the diffusion coefficient increases for curves from left to right: $d_{\mathrm{Re}}=0.5d_{\mathrm{Im}}$, $d_{\mathrm{Re}}=d_{\mathrm{Im}}$, $d_{\mathrm{Re}}=1.5d_{\mathrm{Im}}$, $d_{\mathrm{Re}}=2d_{\mathrm{Im}}$.

responding curve. A further increase of the pump parameter leads to more complicated dynamical regimes.

Stable LS's cannot be obtained for small values of diffusion (very wide apertures). The rough condition for the existence of a LS is that diffusion is approximately larger than diffraction: $d_{\mathrm{Re}}\geqslant d_{\mathrm{Im}}$. For dominating diffraction the stability region of LS shrinks to zero, and periodically pulsing LS's occur.

For $d_{\mathrm{Re}}>d_{\mathrm{Im}}$ the LS's are relatively stable both in the bistability regime (for $p<1$ in Fig. 8), and also in the monostable regime (for $p>1$). In the bistable regime a LS can be written and erased; in the monostable regime one LS always exists. The width of the LS is dependent on the gain parameter p, and is restricted both by d_{Re} and d_{Im} (by the larger one of the two).

Large gain parameters lead to nonstationary LS's. Figure 9 shows nonstationary dynamics of LS's. During the evolution, the field of the LS remains localized; however, the form of the LS changes periodically. At the border between the stationary and nonstationary regime (at the very onset of the nonstationary regime), the width of the LS changes periodically [Fig. 9(a)]. Further increase of the gain leads to complicated periodical branching of LS's: the LS's broadens, splits into two LS's, then one of two LS's wins in the competition, and leads to the new branching cycle [Fig. 9(b)].

With a decrease of d_{Re} (broader aperture of diaphragm in the focal plane) the parameter range corresponding to stable LS shrinks (left curve in Fig. 8). For $d_{\mathrm{Re}}\ll d_{\mathrm{Im}}$, when the diffraction dominates over diffusion, stable LS's are impossible, as follows from our numerical calculations.

The nonstationary dynamics in two dimensions is qualitatively the same. The spot flattens, degenerates into a ring, then the ring splits into two (or sometimes three, or four) LS's, and only one ''daughter'' LS survives in the competition for their common population inversion. The detailed analysis of the nonstationary regimes is outside the scope of the paper, and will be given elsewhere.

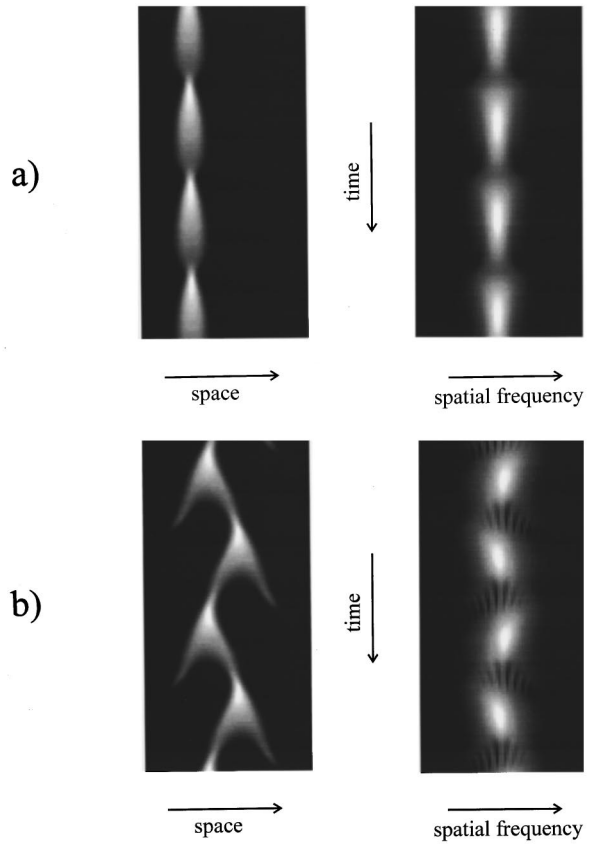

FIG. 9. Nonstationary dynamics of LS's as obtained by numerical integration of Eq. (5) in the case of one spatial dimension: (a) pulsating LS's close to the instability boundary $d_{\mathrm{Im}}=0.5\times10^{-4}$; (b) periodically branching LS's for $d_{\mathrm{Im}}=0.25\times10^{-4}$. The space-time plots are on the left; the Fourier spectrum evolution, at the right. The parameters are $p=0.7$, $d_{\mathrm{Re}}=0.6\times10^{-4}$; the other parameters as in Fig. 8. Time runs over $\Delta t=125$ from the top to the bottom of the plots.

V. DYNAMICS OF LOCALIZED STRUCTURES

A. Switching processes of the localized structures

The quasi-self-imaging resonator geometry leads to dynamical peculiarities of LS's, compared to those of quasiplanar resonators. One such peculiarity (as shown in the previous section) is the strong competition between the LS's. The LS's compete even when they are strongly spatially separated in the near field, which is different from the quasiplanar case where there is not near and far field.

The switching is observed experimentally when the writing laser beam initiates a LS in a new position (Fig. 10): the

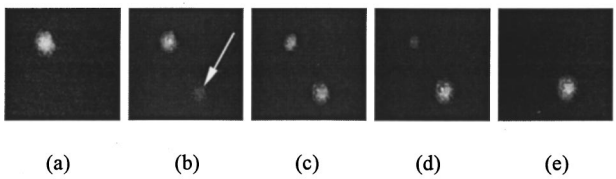

FIG. 10. Switching of LS's initiated by an external bleaching beam in a new position across the laser aperture. Arrow in (b) indicates the place of the initiating beam incidence. The time interval between neighboring pictures is 2.5 s.

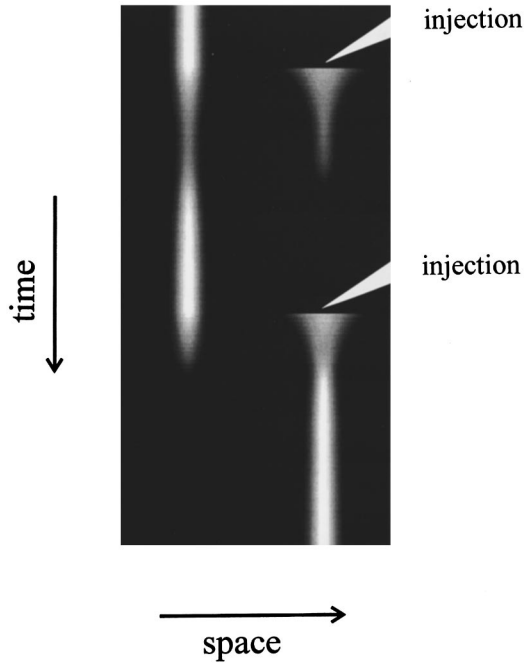

FIG. 11. The dynamics of switching of LS's by injection as obtained by numerical integration of Eq. (5) in case of one spatial dimension. First, injection flash occurs at $t=40$; second, at $t=80$. The peak amplitude of the first injection beam was 4.1; that of the second was 4.4; the width of the injection beam was $\Delta r=0.1$. (For comparison, the peak amplitude of the LS under these conditions was $A_{\text{peak}}=4.882$; the width was $\Delta r=0.0745$.) The parameters are $p=0.8$, $d_{\text{Re}}=1.5\times10^{-4}$, $d_{\text{Im}}=10^{-4}$; the other parameters are as in Fig. 8. Time runs over $\Delta t=125$ from the top to the bottom of the plot.

new soliton is switched on in a new position while the old soliton dies at the same time. This shows the strong competition between the spatial solitons, and implies that a LS can be switched off (erased) by injection anywhere in the absorber plane.

The numerical calculations presented in Fig. 11 illustrate this switching process. In Fig. 11 the simulated injection beam has been switched on twice for a short time. After the injection has been switched on and off for the first time, the initial LS remains, although perturbed by injection. The injection energy (intensity times duration) was not large enough to bleach stronger than at the previous soliton location.

The energy of injection switched on an off for the second time in Fig. 11 is sufficiently strong to win: The initial LS decays, and the new one, induced by injection, develops. The injection energy was 5% larger than in the previous case.

B. Propagation of localized structures in the misaligned resonator

The LS's are stationary for spatially homogeneous parameters (apart from the Brownian motion due to noise). For spatially inhomogeneous parameters, motion of LS's can occur. Such inhomogeneity can, e.g., occur due to a tilt of mirrors and/or lenses in the resonator. Then the space isotropy is broken, and the LS starts to drift (e.g., along the x axis if the resonator mirrors are tilted in the x direction) until they reach the edge of the laser aperture.

The spatial soliton drifts without change in its size or shape when the resonator mirror is tilted [Fig. 12(a)] like that observed in Ref. [5], and predicted in Ref. [12]. In this arrangement, the drift direction is completely determined by the direction of the mirror tilting: when the mirror is tilted around the vertical axis the spatial soliton drifts in the horizontal direction. However, when one of the intracavity lenses is placed closer to the resonator center (see Fig. 1), the spatial soliton drifts even for perfectly aligned resonator mirrors. In this case, the spatial soliton drifts toward the resonator axis independent of its initial location and remains stable on the resonator axis [Fig. 12(b)]. This corresponds to localizing (trapping) of a soliton due to phase troughs [7].

We accounted for the spatial anisotropy by including phenomenologically, the symmetry breaking term in Eq. (5a):

$$\partial_t A=-\vec{k}_{\text{tilt}}\vec{\nabla}A+(d_{\text{Re}}+id_{\text{Im}})\nabla^2A+T_{\text{NL}}. \tag{10}$$

Here, the T_{NL} are the same nonlinear terms as in Eq. (5a). $\vec{k}_{\text{tilt}}$ describes the tilt of the mirror, and has the dimension of a velocity.

The LS's move with a constant velocity proportional to $\vec{k}_{\text{tilt}}$. In the limit of a fast nonlinear absorber: $\gamma\to\infty$ the velocity is equal to $\vec{k}_{\text{tilt}}$; For a slow absorber, the velocity is dependent also on γ. However the slowness of the absorber

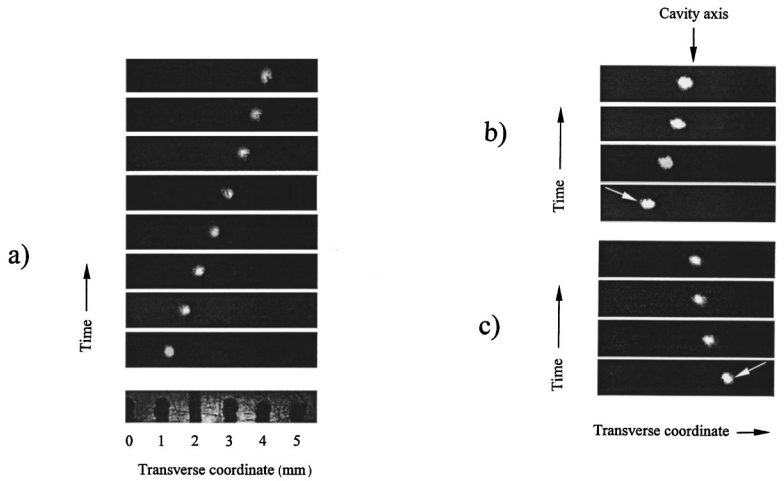

FIG. 12. Drift motion of the LS (a) transversely, for the tilted resonator mirror; (b) and (c) toward the LSA resonator axis for an intracavity lens shift from the self-imaging geometry. Arrows indicate initial positions of the spatial soliton (b) on the left and (c) on the right side of the laser cross section. The time interval between neighboring pictures is 3 s.

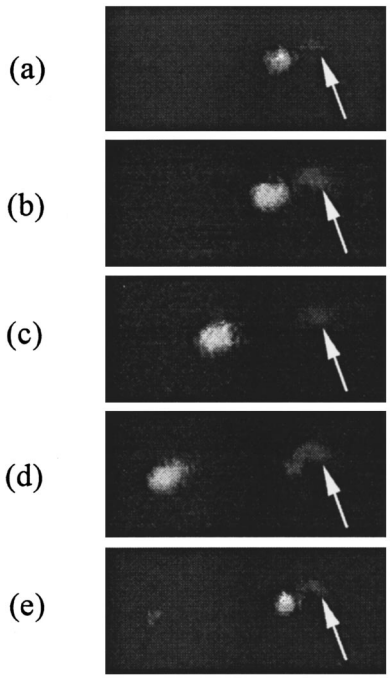

FIG. 13. The periodic LS. Unidirectional drift motion and switching off occurs for a tilted resonator mirror and the permanent local bleaching of the BR absorber cell by a laser beam.

does not produce qualitative differences, thus we give results of the calculation for the case $\gamma \to \infty$ only.

C. Dynamics of localized structures in the misaligned resonator in the presence of constant bleaching

The simultaneous tilt of a laser mirror and the constant injection of the absorber by an external light beam can lead to periodic dynamics. This was observed experimentally: periodic spatial soliton switching on, unidirectional drift motion, and switching off occur (see Fig. 13).

The injection creates a LS at some position. Due to mirror tilt this structure moves away from the bleaching beam position. The bleaching now cannot create a new LS, due to strong competition (as described in the previous subsection). However, when the LS reaches the edge of the resonator mirror (zero boundaries) it dies because of larger losses there. After that, the LS disappears and the injection can create a new one. This scenario is plotted in Fig. 14(a) as obtained numerically.

When, however, the tilt of the mirror is smaller than some threshold, then the LS's can ''glue'' to the edge of the resonator when approaching it. This case is illustrated by a space-time plot in Fig. 14(b).

We can interpret the gluing of a LS to the edge of the resonator in terms of a LS interaction with its image. The edge of the resonator corresponds to zero boundary conditions. The zero boundary can be described by the image of the LS placed symmetrically with respect to the boundary, and with opposite phase to the real structure (the phase of the image is shifted by π). The LS interacts with its image. For zero boundary conditions, this interaction seems to be repulsive, which explains qualitatively the gluing phenomenon.

VI. CONCLUSIONS

We have investigated theoretically and experimentally the emission of a laser with saturable absorber in the form of a spatial soliton. The parameters for the existence of these solitons were determined.

The motivation for these investigations was to prove that LS's can be manipulated, as it is necessary to realize an associative memory as theoretically described in Ref. [7]. Here we have used amplifier and absorber in Fourier-conjugated planes in order to limit the number of LS's to one: to create a simple situation for experimenting with LS's. For excitation of several LS's one has to arrange amplifier and absorber in the same plane. Our first experiments of this kind yielded up to 20 stationary LS's.

The principle results of the work are the proofs that solitons are bistable. A soliton can be written anywhere in the laser cross-section (spatial multistability). Solitons remain structurally stable in the presence of phase gradients. They drift along a phase gradient, and they can be captured by a phase trough. And finally, good correspondence between experiments and numerical simulations may be mentioned.

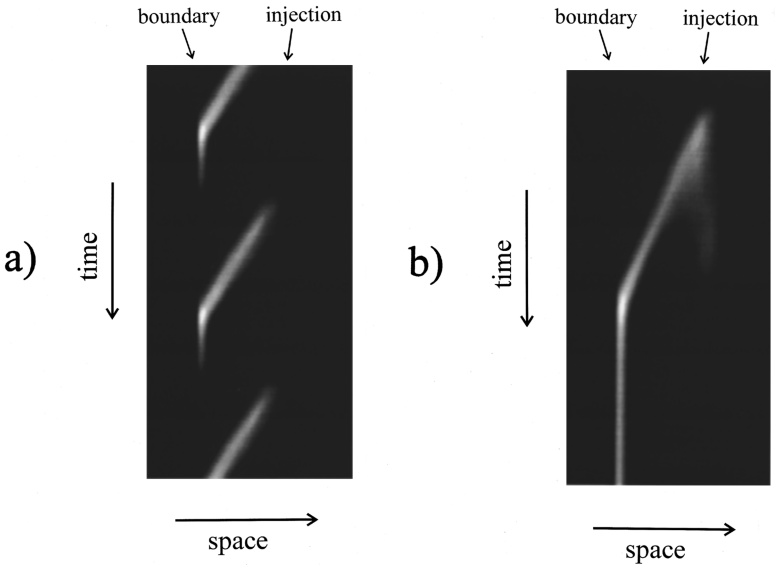

FIG. 14. (a) Periodic switching of the LS in the presence of constant injection and tilted mirrors as obtained by numerical integration of Eq. (5) in the case of one spatial dimension for relatively large tilt, $k_{\text{tilt}}=0.01$; (b) ''gluing'' of the LS to the edge of the resonator for smaller tilt $k_{\text{tilt}}=0.005$. The parameters of injection beam are peak amplitude, $A_{\text{peak}}=2.5$; width, $\Delta r=0.1$; other parameters as in Fig. 8. Time runs over $\Delta t=125$ from the top to the bottom of the plot.

ACKNOWLEDGMENTS

We acknowledge discussions with M. Vaupel, G. Slekys, M. S. Soskin, and V. Yu. Bazhenov. This work has been supported by ESPRIT LTR Project ''PASS,'' Deutsche Forschungsgemeinschaft under Grant No. WE-743/9-2, and BMFT Grant No. X272.4.

[1] M. Tlidi and P. Mandel, Chaos Solitons Fractals **4**, 1475 (1994); A. J. Scroggie and W. Firth, *ibid.* **4**, 1323 (1994); P. Mandel and T. Erneux, Opt. Commun. **44**, 55 (1982); L. A. Lugiato and C. Oldano, Phys. Rev. A **37**, 3898 (1988); M. Tlidi, Paul Mandel, and R. Lefever, Phys. Rev. Lett. **73**, 640 (1994).

[2] H. R. Brand and R. J. Deissler, Physica A **204**, 87 (1994); N. N. Rosanov, Prog. Opt. **35**, 1 (1996).

[3] K. Staliunas and Víctor J. Sánchez-Morcillo, Opt. Commun. (to be published); Stefano Longhi, Phys. Scr. (to be published).

[4] V. Yu. Bazhenov, V. B. Taranenko, and M. V. Vasnetsov, Proc. SPIE **1840**, 183 (1992).

[5] M. Saffman, D. Montgomery, and D. Z. Anderson, Opt. Lett. **19**, 518 (1994).

[6] R. Neubecker, G.-L. Oppo, B. Thüring, and T. Tschudi, Phys. Rev. A **52**, 791 (1995).

[7] W. J. Firth and A. J. Scroggie, Phys. Rev. Lett. **76**, 1623 (1996).

[8] J. Soppa and D. Oesterhelt, J. Bio. Chem. **264**, 13 043.

[9] D. Oesterhelt and W. Stoekenius, Nature **233**, 149 (1971); D. Oesterhelt and W. Stoekenius, Proc. Natl. Acad. Sci. USA , **70**, 2853 (1975).

[10] *Biopolymers for Real-Time Optical Processing, Optical Processing and Computing*, edited by V. Yu. Bazhenov, M. S. Soskin, V. B. Taranenko, and M. V. V. Vasnetsov (Academic Press, Boston, 1989); N. Hampp, C. Brauchle, and D. Oesterhelt, Biophys. J. **58**, 83 (1990); R. R. Birge, Annu. Rev. Phys. Chem. **41**, 683 (1990).

[11] e.g., Anthony E. Siegman, *Lasers* (University Science Books, Mill Valley, California, 1986).

[12] M. Haelterman and G. Vitrant, J. Opt. Soc. Am. B **9**, 1563 (1992).